Theor Chem Acc (2012) 131:1216
DOI 10.1007/s00214-012-1216-9

REGULAR ARTICLE

Ab initio parametrized polarizable force field for rutile-type SnO_2

Wojciech Miiller · Gordon J. Kearley · Chris D. Ling

Received: 19 February 2012 / Accepted: 30 March 2012 / Published online: 17 April 2012

Abstract We report a new, polarizable classical force field for the rutile-type phase of SnO_2, casserite. This force field has been parametrized using results from ab initio (density functional theory) calculations as a basis for fitting. The force field was found to provide structural, dynamical and thermodynamic properties of tin oxide that compare well with both ab initio and experimental results at ambient and high pressures.

Keyword Tin dioxide · SnO2 · Molecular dynamics · Force field parametrization · Ab initio · DFT

1 Introduction

Ab initio calculations on solid-state materials are becoming increasingly routine through the use of plane-wave methods in density functional theory (DFT). They can help solve and verify complex structures in combination with potentially ambiguous crystallographic data [1] and are often crucial to the interpretation of spectroscopic data [2]. However, there are many systems of great experimental interest and applied significance that remain intractable to DFT due because its relatively heavy computational cost does not permit a sufficient size of unit cell and/or timescale of dynamics simulations. These include: the modelling of nanoscale structural (dis)order to help interpret experimental diffuse scattering data from, for example, lead-free relaxor ferroelectrics [3]; and the modelling of ionic conduction mechanisms to help interpret inelastic neutron scattering data from, for example, solid-state fuel cell or lithium-ion battery materials [4]. Such problems can only be approached with "classical" atomistic methods. The accuracy of these methods depends heavily on the reliability of the force fields used. Unfortunately, if a system of interest contains atomic species that have not been widely subjected to these methods and/or for which a large amount of experimental data are not available, the development and exhaustive testing of force fields can be a prohibitive task. A potential way of speeding up (or even automating) this process is to use observables including forces, potential energies and strain tensor elements from high-precision DFT "experiments" on manageably small unit cells or timescales to parameterize classical force fields that can subsequently be used to run calculations on much larger unit cells or timescales - thus "bridging the gap" between ab initio and classical methods. There were reported ab initio parametrized force fields for relatively simple oxides as SiO_2 [5], TiO_2 [6], GeO_2 [7] and more complex materials as $BaTiO_3$ [8], $PbTiO_3$ and $PbMg_{1/3}$ $Nb_{2/3}O_3$. [9].

Tin(IV) oxide has attracted considerable interest due to its extraordinary electronic, optical and catalytic properties. Of particular significance is its potential for applications in displays, solar cells and optoelectronic devices, due to its being simultaneously transparent and electrically conducting[10]. It is also a prospective material for gas sensors and rechargeable batteries applications [11, 12].

At ambient pressure, tin oxide crystallizes in the rutile structure ($P4_2/mnn$ symmetry), shown in Fig. 1 and undergoes series of structural transitions under pressure. Those observed experimentally are the following: rutile

W. Miiller (✉) · C. D. Ling
School of Chemistry, The University of Sydney, Sydney, NSW 2006, Australia
e-mail: w.miiller@chem.usyd.edu.au

W. Miiller · G. J. Kearley
Braggs Institute, ANSTO, Locked Bag 2001, Kirrawee DC, NSW 2232, Australia

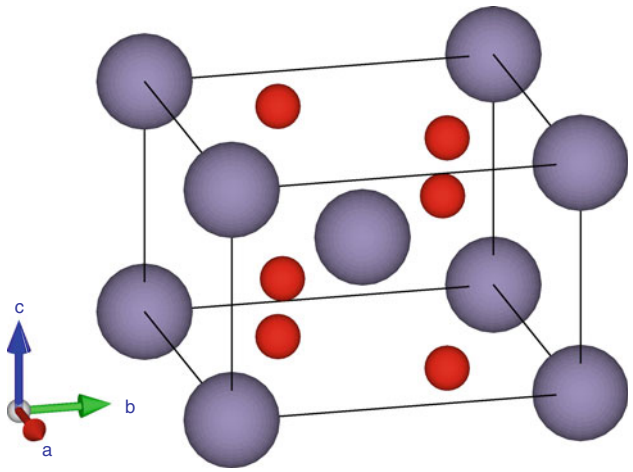

Fig. 1 Rutile-type SnO_2 tetragonal primitive cell. Large (*violet*) and small (*red*) spheres represent Sn cations and O anions, respectively

($P4_2/mnn$) → $CaCl_2$-type ($Pnnm$) → pyrite-type ($Pa\bar{3}$) → → orthorhombic ZrO_2-type ($Pbca$) → cottunite-type ($Pnam$) [13, 14]. As SnO_2 is a relatively simple material, this remarkable variety of highly coordinated phases under pressure creates additional interest.

Theoretical investigation into all these phases has been conducted within various theoretical approximations. Density functional theory (DFT)-derived structural, electronic and mechanical properties compare favorably with experiment [15–17]. DFT-based methods have a high demand on computing resources that limits number of atoms to less than about 1000 over timescales of only a few tens of picoseconds. To perform large-scale molecular dynamic (MD) simulations dealing with hundreds of thousands of molecules over with longer timescales, much faster classical force fields are required. However, parameterizing classical force fields sufficiently well to yield reliable results is often a prohibitive task. One approach is to use ab initio-derived observables including forces, potential energies and strain tensor elements for parametrization.

In this report, we propose a novel, polarizable interatomic force field, parametrized from ab initio results. Its reliability was tested by calculation of structural, dynamical and thermodynamic properties of the rutile phase of SnO_2. Our force field was found to describe SnO_2 reliably at ambient and high pressures.

This introduction is followed by the force field details (Sect. 2), the parametrization procedure (Sect. 3), the force field tests (Sect. 4) and a summary (Sect. 5)

2 Force field

A force field describes the potential energy acting on ions in a crystal lattice as a set of functions. Short-range dispersive forces are simulated using the pairwise Morse-stretch potential:

$$E_{sr} = D_{ij}[e^{\gamma_{ij}[1-r_{ij}/\rho_{ij}]} - 2e^{\gamma_{ij}/2[1-r_{ij}/\rho_{ij}]}] \quad (1)$$

where $r_{ij} = \mid r_i - r_j \mid$ is the distance between i and j ions and D_{ij}, γ_{ij} and ρ_{ij} are pairwise parameters. We have truncated this potential at the 10 Åcutoff radius.

The term describing the electrostatic contribution to the total energy of the system consists of charge–charge, charge–dipole and dipole–dipole contributions. The Wolf summation was used for calculation of Coulomb interactions, (described in detail in [18, 19]), with a cutoff of 13 Å. It was found that an Ewald parameter of $\kappa = 0.1$ was sufficient.

In addition to the Morse-stretch and Coulomb interactions, we have included the effects of dipole polarization on both O and Sn ions. According to the Tangney-Scandolo model [5], the induction of dipole moments can be due to both by electrostatic forces and the short-range repulsive forces between anions and cations. The latter contribution is given by formula proposed by Madden et al. [20]

$$p_i^{sr} = \alpha_i \sum_{j \neq i} \frac{q_j r_{ij}}{r_{ij}^3} f_{ij}(r_{ij}) \quad (2)$$

where

$$f_{ij}(r_{ij}) = c_{ij} \sum_{k=0}^{4} \frac{(b_{ij} r_{ij})^k}{k!} e^{-b_{ij} r_{ij}} \quad (3)$$

where α_i is the polarizability of species i and b_{ij} and c_{ij} are model parameters.

The total dipole moment can be found in an iterative way, such that p_i^n on atom i and iteration step n is

$$p_i^n = \alpha_i E(r_i; \{p_j^{n-1}\}_{j=1,N}, \{r_{jj=1,N}\}) + p_i^{sr} \quad (4)$$

where E is the electric field, calculated from the dipole moments and charges in previous steps. These force fields are included in the IMD (ITAP Molecular Dynamics Program) package, developed at the University of Stuttgart, Germany [21].

The resulting force field consists of 19 parameters: pairwise D_{ij}, γ_{ij}, ρ_{ij}, b_{ij}, c_{ij}, charges q_i and polarizabilities α_i associated with ion type. To conserve the neutral character of the crystal, we used the relation $q_{Sn} = -2q_O$, so that the effective number of variables used in parametrization was 18. The complex form of the potential is necessary for good reproduction of DFT observables.

3 Force field parametrization

The parameters of the force field described in detail in the previous section were determined as follows. We have

fully optimized three 2 × 2 × 3 supercells of rutile SnO_2 using the Vienna ab initio Simulation Package [22] (VASP in version 5.2). One supercell was optimized at zero pressure, and two other were optimized using 4 % higher and lower molar volumes. We used standard Generalized Gradient Approximation pseudopotentials (GGA) [23] for both O and Sn with 2 × 2 × 2 *k*-mesh and 600 eV energy cutoff for the convergence of the strain tensor elements. Forces and energies were optimized to 5×10^{-6} eV $Å^{-1}$ and 10^{-7} eV, respectively.

The parameterization procedure of the classical force field is illustrated schematically in Fig. 2. Ab initio MD with a 220 eV energy cutoff and using only the Γ(0, 0, 0) point in reciprocal space was performed over 10,000 steps with a 3 fs timestep for all three supercells at 600 K. This was to provide a large number of non-correlated physically plausible atomic configurations from which configurations were selected as follows: For all three optimized supercells plus five random configurations from the ambient pressure run and one additional random frame from the smaller and larger volumes, the forces acting on ions, total energies and strain tensor elements were calculated using the same settings as for structure optimization. A database was constructed consisting of these values, which was used as a reference for force field parametrization. Higher and lower volume supercells were used to explore a larger range of configurational space. For the same snapshot structures, we constructed input files for the classical MD code, although no MD was actually performed, only a single-point energy calculation. However, the classical approach requires larger cells, so we multiplied the cell by 2 in each direction.

Since parametrization aims to reproduce the ab initio observables by a classical force field, a cost function should be constructed that can be minimized indirectly by adjusting the force field parameters. We chose a cost function based on root-mean-squared-error values:

$$f = \frac{\sqrt{\sum_{k=1}^{K}\sum_{n=1}^{N}\sum_{a} \mid F_{ai,n,a}^{k} - F_{cl,n,a}^{k} \mid^{2}}}{\sqrt{\sum_{k=1}^{K}\sum_{n=1}^{N}\sum_{a}(F_{ai,n,a}^{k})^{2}}} \tag{5}$$

$$e = \frac{\sqrt{\sum_{k,l=1}^{K}\left((E_{ai,k} - E_{ai,l}) - (E_{cl,k} - E_{cl,l})\right)^{2}}}{\sqrt{\sum_{k,l=1}^{K}(E_{ai,k} - E_{ai,l})^{2}}} \tag{6}$$

$$s = \frac{\sqrt{\sum_{k=1}^{K}\sum_{ab} \mid S_{ai,ab}^{k} - S_{cl,ab}^{k} \mid^{2}}}{\sqrt{\sum_{k=1}^{K}\sum_{ab}(S_{ai,ab}^{k})^{2}}} \tag{7}$$

where $F_{n,a}^{k}$ is the *a*-th component (*x*, *y* or *z*) of the force acting on *n*-th atom in the *k*-th frame. E_k is total energy of *k*-th frame atomic configuration, and S_{ab}^{k} is element *ab* (*a*, *b* = *x*, *y* or *z*) of the strain tensor of frame *k*. The indices *ai* and *cl* refer to VASP and classical MD-derived values, respectively. The cost function should consist of all three components with properly chosen weights:

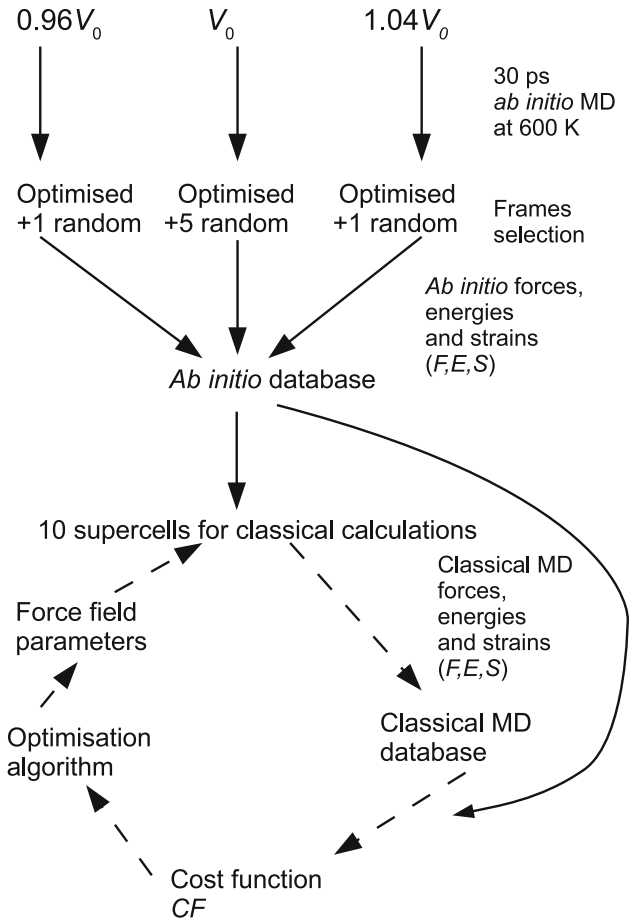

Fig. 2 Sketch of parametrization procedure. Dashed arrows indicate iterative minimization of the cost function *CF*

$$CF = w_f f + w_s s + w_e e \tag{8}$$

and $w_f > w_s > w_s$, as we have many more forces than strain tensor elements and energies in the database for comparison. In the formula for *e*, the relative difference between configurational energies of different snapshots was considered, as the forces depend only on the gradient of energy, not its absolute values.

The parametrization problem can be treated as a classical black box problem-its properties can be viewed only in terms of input (force field adjustable parameters) and output (the cost function). A number of algorithms have been developed for the optimization of such black boxes. In the present case, we used a genetic algorithm based on the Covariance Matrix Adaptation Evolution Strategy [24] (CMAES) for the initial set of parameters, followed by a Mesh Adaptive Direct Search (MADS, implemented to NOMAD [25] package) algorithm [26]. The IMD MD package was interfaced with these programs using perl [27] scripts. At every optimization step, a cost function was

calculated, and a new set of parameters generated to minimize it. This approach, based on modular scheme and sequential procedure, makes this method very flexible and easily transferable to different classical MD codes, slightly modifying scripts.

Approximately 80,000 iterations were required to obtain a cost function value of $CF = 0.13995$ with $f = 0.08083$, $e = 0.03846$ and $s = 0.11056$. This means that the root errors of forces, energies and strain elements are lower than 12 %, indicating very close agreement between ab initio and classical MD quantities. Figure 3 shows comparison of ab initio and classically derived forces for a random MD snapshot. The resulting force field parameters are collected in Table 1.

4 Force field tests

4.1 Structural and mechanical properties

The zero-pressure structural parameters for the SnO_2 rutile structure obtained using DFT and the new force field are shown in table [2] together with experimental values. The tetragonal rutile structure invokes only three "free" parameters: the lattice constants a, c and one Wyckoff coordinate x. DFT, as usual, yields overbonding and smaller volumes, this being a consequence of imperfect exchange-correlation potential treatment. Agreement between DFT-derived lattice parameters and those obtained using the classical force field is very good. The force field reproduces $P4_2mnn$ symmetry operations to an accuracy better than 5×10^{-6} Å.

Figure 4 shows energy as a function of volume calculated using GGA and the new force field. The agreement between both curves is very good, as reflected in an analysis of the Birch–Murnagham equation of state [28]:

$$E = \frac{9V_0B_0}{16}\left[\left[\left(\frac{V_0}{V}\right)^{2/3} - 1\right]^3 B_0^* + \left[\left(\frac{V_0}{V}\right)^{\frac{2}{3}} - 1\right]^2 \left[6 - 4\left(\frac{V_0}{V}\right)^{\frac{2}{3}}\right]\right] + E_0 \quad (9)$$

where V, V_0, E, E_0, B_0, B_0* stand for volume, equilibrium volume, energy, equilibrium energy, the bulk modulus and its pressure derivative, respectively. The resulting parameters are shown in Table 2 with experimental data. The agreement with both LDA and experimental results is remarkably good. Ab initio-derived values of bulk modulus and its pressure derivative B* are in very good agreement with previous theoretical studies [16].

Figure 5 shows the pressure dependence of the reduced lattice parameters and molar volume, taken from ref. [13]. These characteristics are well reproduced by both our force field and GGA, especially the reduced compressibility of SnO_2 along the c-axis.

Elastic constants (*aka* elastic moduli) are parameters that define properties of the material undergoing stress and deformation. Elastic moduli are given by the relation: $C_{ijkl} = \sigma_{ij}/\epsilon_{lk}$, where σ_{ij} stands for strain and ϵ_{kl} for relative deformation. The agreement between our potential, GGA and available experimental results is rather good, as shown in Table 3.

4.2 Vibrational, electronic and thermodynamic properties

In polar dielectric crystals, a macroscopic electric field is exerted by longitudinal phonons. This electric field is responsible for the well-known phenomenon of LO-TO phonon splitting at the Brillouin zone center, Γ point. Born effective charges, Z^*, are a measure of coupling between phonons and this electric field. These charges can be estimated using displacements of anion and cation sublattices:

$$Z^* = \frac{\partial P_i}{e\partial\rho_j} \quad (10)$$

where P stands for polarization, ρ for displacement of the ion, e is the elemental charge and $i, j = x, y, z$. Resulting effective charges for our potential are $Z^*_{Sn\text{-}xx} = -2Z^*_{O\text{-}xx} = 2.603$, $Z^*_{Sn\text{-}zz} = -2Z^*_{O\text{-}zz} = 2.688$, and off-diagonal elements of the Z^* tensor are 0. The resulting values of Z^* are much lower than predicted by ab initio methods, which yield $Z^*_{Sn\text{-}xx} = Z^*_{Sn\text{-}yy} = -4.20$, $Z^*_{O\text{-}xx} = Z^*_{O\text{-}yy} = -2.09$, $Z^*_{Sn\text{-}zz} = -2Z^*_{O\text{-}zz} = 4.62$, $Z^*_{Sn\text{-}xy} = 0.54$ and $Z^*_{O\text{-}zz} = -0.77$ [16]. This disagreement is not surprising, as electronic properties were not included in

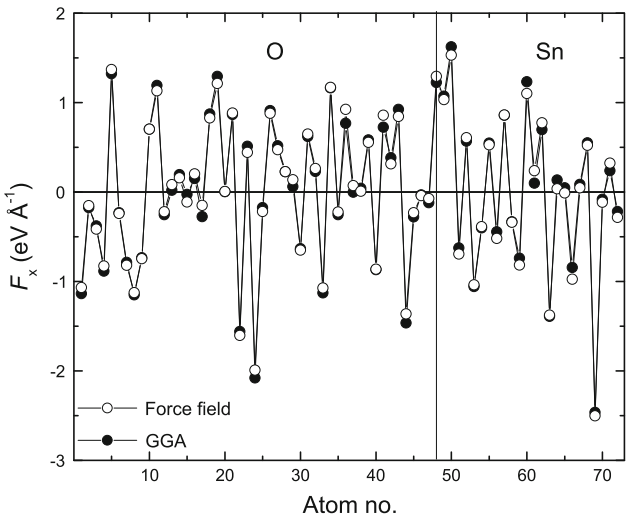

Fig. 3 Comparison of x-component of forces acting on 48 O and 24 Sn ions in one of the MD frames, calculated with GGA and our force field

Table 1 Force field parameters for the rutile structure of SnO_2

	O	Sn	O–O	O–Sn	Sn–Sn
D (eV)			4.41×10^{-3}	2.38709×10^{-4}	1.3624×10^{-1}
γ			12.47595	17.4598	28.758545
ρ (Å)			3.77486	3.8856	3.04968
q (e)	−1.27917	2.55834			
α (Å V^{-1})	3.714×10^{-2}	3.18×10^{-7}			
b ($Å^{-1}$)			1.98313	5.63211	48.35819
c (eV $Å^{-1}$)			7.97238	−148.22664	-25.5×10^{3}

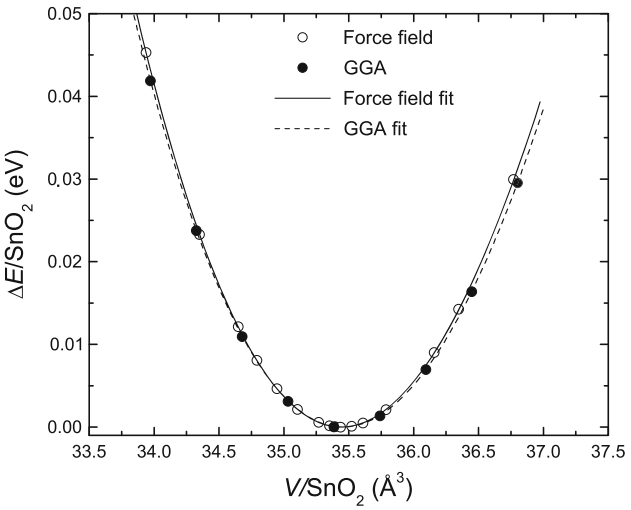

Fig. 4 $\Delta E(V)$ derived from GGA and classical MD calculations. Solid lines are fit to Eq. 9

our cost function used for potential parametrization. However, the non-analytical term in the dynamical matrix arising from the macroscopic electric field is proportional to the $Z_1^* Z_2^*/\epsilon$ ratio [31], where ϵ is the electronic dielectric constant, calculated using small electric fields:

$$Z^* = \delta_{ij} + \frac{4\pi}{\epsilon_0}\frac{\partial P_i}{\partial E_j} \tag{11}$$

where E stands for electric field, ϵ_0 is the vacuum permittivity and δ_{ij} is the Kronecker's delta. The values given by the force field are $\epsilon_{xx} = \epsilon_{yy} = 1.314$ and $\epsilon_{zz} = 1.305$, much smaller then DFT mean value of 4.95 [16]. The resulting values $Z^*_{Sn-xx}/\sqrt{\epsilon_{xx}} = -2Z^*_{O-xx}/\sqrt{\epsilon_{xx}} = 2.271$ and $Z\text{-}yy^*/\sqrt{\epsilon_{yy}}$, $Z^*_{Sn-zz}/\sqrt{\epsilon_{zz}} = -2Z^*_{Sn-zz}/\sqrt{\epsilon_{zz}} = 2.354$ are in good agreement with those previously reported $Z^*_{Sn}/\sqrt{\epsilon} = -2Z^*_0/\sqrt{\epsilon} = 1.98$ [17] and $Z^*_{Sn}/\sqrt{\epsilon} = -2Z^*_0/\sqrt{\epsilon} = 1.888$ [16].

A comparison of the phonon dispersion via the special points $\Gamma(0,0,0), X(\frac{1}{2},0,0), Z(0,0,\frac{1}{2}), M(\frac{1}{2},\frac{1}{2},0), R(\frac{1}{2},0,\frac{1}{2})$ and $A(\frac{1}{2},\frac{1}{2},\frac{1}{2})$ in the Brillouin zone, calculated using our potential and GGA, is displayed in Fig.6. Phonons were determined using a small displacement method in $2 \times 2 \times 3$ (GGA) and $6 \times 6 \times 8$ (force field) supercells analyzed using PHONON package[32]. The Ab initio data are in excellent agreement with published data [17]. The force field reproduces all the main features of GGA dispersion, especially at lower frequencies ($\omega < 10$ GHz), but slightly overestimates the higher frequency vibrations in the $M - X$ direction and slightly alters the Γ-centered optical modes. SnO_2 at pressures below 11 GPa undergoes a ferroelastic transition to the $CaCl_2$-type structure. According to Parliński and Kawazoe [17], the main mechanism responsible for this phenomenon is based on the softening of the B_{1g} optical mode (indicated with an arrow in Fig. 6). We therefore calculated Γ-point frequencies of B_{1g} mode at several pressures using our potential, and indeed, this mode softens as expected (Fig. 7a). The value of the Grüneisen parameter, $v = -(\partial \ln \omega/\partial \ln V)$ given by our force field is $v(B_{1g}) = -15.06$ (fit is shown in Fig. 7a), in very good agreement with the LDA value −14.17 [17] and comparable to the experimental value −10.44 [33].

We were able to estimate the thermal expansion coefficient of SnO_2 with our force field approximation using $\alpha_V = \partial \ln V/\partial T = 16.2 \times 10^{-6}$ after a series of NPT calculations on the 1728 atom supercells at various temperatures (derived $V(T)$ dependence is shown in the inset of Fig. 7b together with experimental data taken from [34]),

Table 2 Structural and equation-of-state parameters for SnO_2, given by our force field, GGA and experiment

	a	c	x	V_0/SnO_2 ($Å^3$)	B_0 (GPa)	B_0^*
Force field	4.723	3.1773	0.3056	35.4375	207.7	5.16
GGA	4.7177	3.1798	0.3058	35.3859	199.3	4.98
exp[13]	4.7367	3.1855	0.307	35.7354	205(7)	7.4(2)

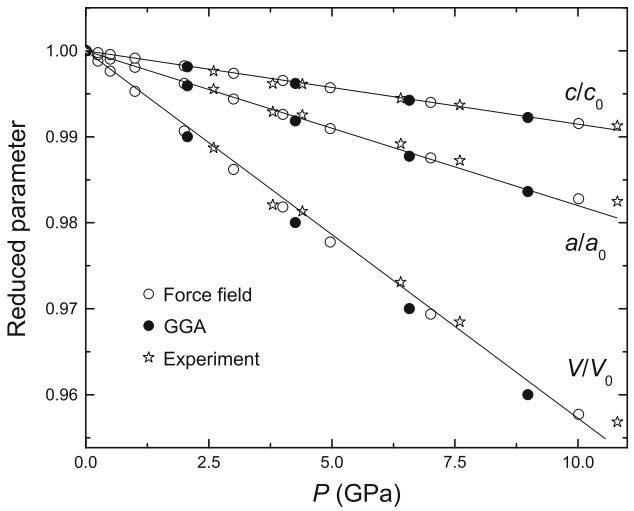

Fig. 5 Pressure dependencies of reduced lattice parameters a, c and molar volume V taken from GGA, MD and available experimental data [13]. Solid lines are guides for the eye

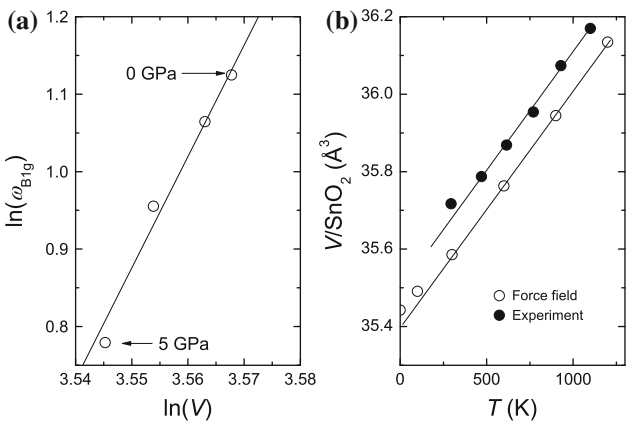

Fig. 7 **a** Grüneisen relation of the B_{1g} phonon frequency ω_{B1g} calculated using our potential. The solid line is a fit (for details see the text). **b** Temperature dependence of the formula unit volume V, derived from our force field in comparison with experimental data [34]. Solid lines are guides for the eye

Table 3 Elastic constants for the rutile structure of SnO_2

	Force field	GGA	exp [29]	exp [30]
C_{11}	269	246.6	261.7	268
C_{12}	190.2	183.4	177.2	173
C_{13}	155.3	156.5	155.5	
C_{33}	474.7	459.6	449.6	
C_{44}	95.4	97.4	103.1	109
C_{66}	181.5	203.27	207.4	207

Values are given in GPa. Indexing is according to the Voigt notation (1, 2, 3, 4, 5, and 6 numbers stand for xx, yy, zz, yz, zx, xy, respectively)

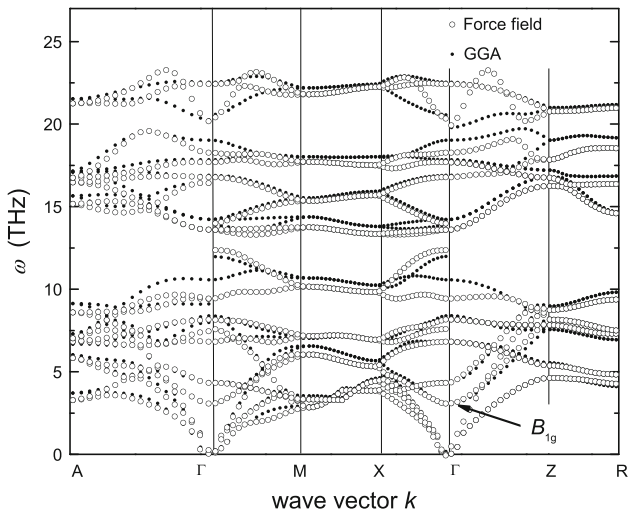

Fig. 6 Phonon dispersion curves from GGA and our force field. An arrow points B_{1g} optical mode

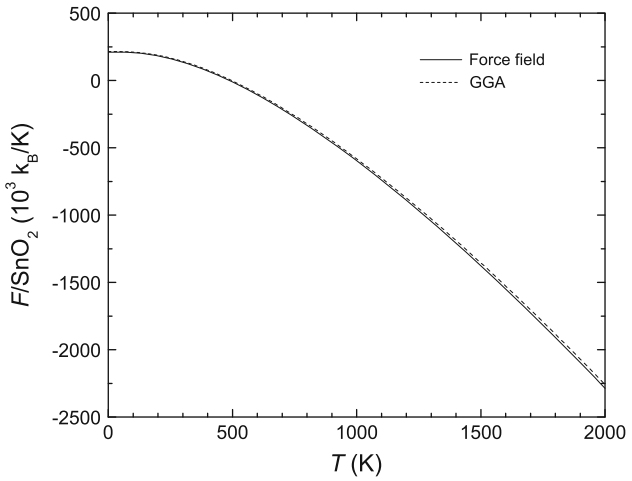

Fig. 8 Free energy F as a function of temperature T, derived from phonon dispersion relations given by GGA and force field

with Nóse-Hoover thermostat and barostat [35, 36]. This value is comparable to the experimental one 11.7×10^{-6} [33].

Phonon dispersion may be used to calculate basic thermodynamic properties: free energy F and constant volume heat capacity, C_V. The temperature dependence of these quantities was calculated within the quasiharmonic approximation, implemented in the PHONON package [32]. The resulting curves for the force field and GGA are shown in Figs. 8 and 9. The agreement between these two approaches is very good-as one can see, the relative offset between GGA and force field-calculated heat capacities is lower than 3% and can be associated with the underestimation of phonon frequencies by the latter model, noticeable in Fig. 6. Calculated free energy $F(T)$ dependencies

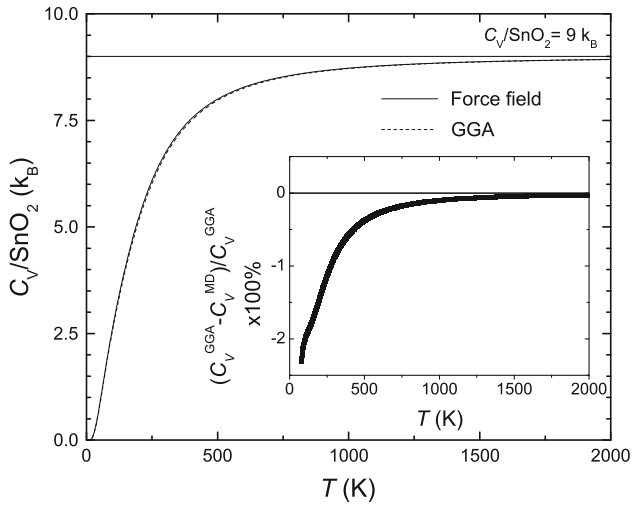

Fig. 9 Temperature dependence of C_V given by our force field and GGA. The inset shows relative difference between both curves

are also well reproduced by our potential. Notice that at temperatures above 1,000 K, C_V tends to saturate at the $9k_B$ value, expected for the Dulong–Petit law.

As experimental estimation of C_V is extremely difficult for solids, one can calculate the heat capacity at constant pressure, C_p, using the formula:

$$C_P = C_V + \alpha_V^2 B_0 V T \tag{12}$$

where α_V is the thermal expansion, B_0 is bulk modulus, V is volume and T is temperature. The resulting $C_p(T)$ dependence, together with experimental data taken from ref. [37], is shown in Fig. 10. As one can see from the inset, the force field overestimates C_p by about 10 % at low temperatures (below 200 K); however, with increasing temperature this disparity decreases.

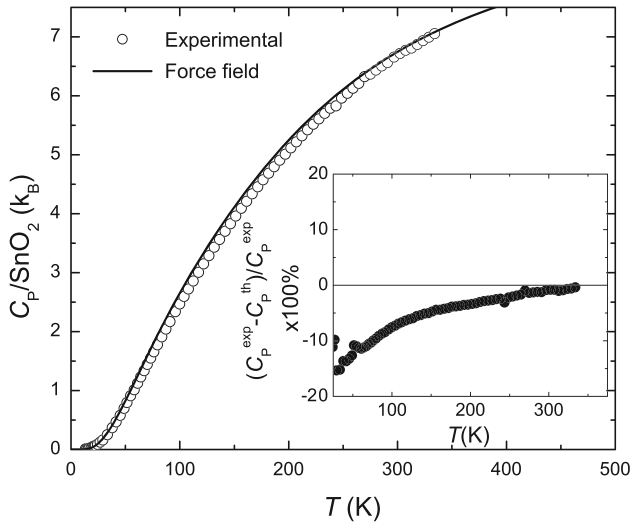

Fig. 10 Temperature dependence of C_p taken from literature [37] and given by our force field. The inset shows the relative difference between the curves

5 Summary

In conclusion, we have developed a classical force field for rutile-type SnO_2, based on ab initio data. We show that this particular potential reproduces DFT-derived features of this material reasonably well, including structure, bulk modulus, elastic constants as well as thermodynamic properties related to vibrational spectra. Additionally, it was shown that this force field is valid at high pressures, reproducing the pressure dependence of the lattice parameters and the B_{1g} mode softening responsible for the experimentally observed ferroelastic phase transition in SnO_2. However, we have to emphasize that the presented potential was developed based on the properties of rutile-type of SnO_2 and should therefore be used only for modeling of this particular phase. We have also presented a fast, almost "automatic" method for force field parametrization, easily transferable between different forms of potentials and classic MD codes.

Acknowledgments Authors would like to acknowledge Dr. Marek Paściak, Australian National University, for fruitful discussion.

References

1. Ling CD, Johnson M (2004) J Solid St Chem 177(6):1838
2. Kearley G, Johnson M (2010) Vib Spectrosc 53(1):54
3. Xu G, Zhong Z, Bing Y, Ye ZG, Shirane G (2006) Nat Mater 5:134
4. Ammundsen B, Burns GR, Islam MS, Kanoh H, Rozićre J (1999) J Phys Chem 103(25):5175
5. Tangney P, Scandolo S (2002) J Chem Phys 117(19):8898
6. Han XJ, Bergqvist L, Dederichs PH, Müller-Krumbhaar H, Christie JK, Scandolo S, Tangney P (2010) Phys Rev B 81:134108
7. Marrocchelli D, Salanne v, Madden PA, Simon C, Turq P (2009) Mol Phys 107:443
8. Tinte S, Stachiotti MG, Sepliarsky M, Migoni RL, Rodriguez CO (1999) J Phys Condens Matter 11(48):9679
9. Sepliarksky M, Wu Z, Asthagiri A, Cohen RE (2004) Ferroelectrics 301:55
10. Chopra K, Major S, Pandya D (1983) Thin Solid Films 102(1):1
11. Idota Y, Kubota T, Matsufuji A, Maekawa Y, Miyasaka T (1997) Science 276(5317):1395
12. Wang Y, Jiang X, Xia Y (2003) J Am Chem Soc 125(52):16176
13. Haines J, Léger JM (1997) Phys Rev B 55:11144
14. Shieh SR, Kubo A, Duffy TS, Prakapenka VB, Shen G (2006) Phys Rev B 73:014105
15. Liu CM, Chen XR, Ji GF (2011) Comput Mater Sci 50(4):1571
16. Borges P, Scolfaro L, Leite Alves H, da Silva E (2010) Theor Chem Acc 126:39
17. Parlinski K, Kawazoe Y (2000) EPJ B 13:679
18. Wolf D, Keblinski P, Phillpot SR, Eggebrecht J (1999) J Chem Phys 110(17):8254

19. Brommer P, Beck P, Chatzopoulos A, Gähler F, Roth J, Trebin HR (2010) J Chem Phys 132(19):194109
20. Wilson M, Madden PA (1993) J Phys Condens Matter 5(17):2687
21. Stadler J, Mikulla R, Trebin HR (1997) IJMPC 8:1131
22. Kresse FJ (1996) G Phys Rev B 54(16):11169
23. Perdew JP, Chevary JA, Vosko SH, Jackson KA, Pederson MR, Singh DJ, Fiolhais C (1992) Phys Rev B 46:6671
24. Hansen N (2006) In: Lozano J, Larranaga P, Inza I, Bengoetxea E (eds.) Towards a new evolutionary computation. Advances on estimation of distribution algorithms. Springer, Berlin, pp 75–102
25. Abramson M, Audet C, Couture G, Dennis J, Le Digabel S. The nomad project. Software available at http://www.gerad.ca/nomad.
26. Le Digabel S (2011) ACM Trans Math Softw 37(44):1
27. The Perl programming language, http://www.perl.org
28. Birch F (1947) Phys Rev 71:809
29. Chang E, Graham EK (1975) J Geophys Res 80:2595
30. Hellwig H, Goncharov AF, Gregoryanz E, Mao HK, Hemley RJ (2003) Phys Rev B 67:174110
31. Pick RM, Cohen MH, Martin RM (1970) Phys Rev B 1:910
32. Parliński K (2006) Software PHONON
33. Peercy PS, Morosin B (1973) Phys Rev B 7:2779
34. Seki H, Ishizawa N, Mizutani N, Kato M (1984) J Ceram Soc Jpn 92:219
35. Nóse S (1984) J Chem Phys 81(1):511
36. Hoover WG (1985) Phys Rev A 31:1695
37. Polyakov V, Mineev S, Clayton R, Hu G, Gurevich V, Khramov D, Gavrichev K, Gorbunov V, Golushina L (2005) Geochim cosmochim Acta 69(5):1287